
This is an electronic reprint of the original article.

This reprint may differ from the original in pagination and typographic detail.

Author(s): Malitckaya, Maria & Komsa, Hannu-Pekka & Havu, Ville & Puska, Martti J.

Title: First-Principles Modeling of Point Defects and Complexes in Thin-Film Solar-Cell Absorber CuInSe₂

Year: 2017

Version: Pre-print

Please cite the original version:

Malitckaya, Maria & Komsa, Hannu-Pekka & Havu, Ville & Puska, Martti J. 2017. First-Principles Modeling of Point Defects and Complexes in Thin-Film Solar-Cell Absorber CuInSe₂. Advanced Electronic Materials. 1600353. ISSN 2199-160X (printed). DOI: 10.1002/aelm.201600353.

Rights: © 2017 Wiley-Blackwell. This is the non peer reviewed version of the following article: Malitckaya, Maria & Komsa, Hannu-Pekka & Havu, Ville & Puska, Martti J. 2017. First-Principles Modeling of Point Defects and Complexes in Thin-Film Solar-Cell Absorber CuInSe₂. Advanced Electronic Materials. 1600353. ISSN 2199-160X (printed). DOI: 10.1002/aelm.201600353, which has been published in final form at <http://onlinelibrary.wiley.com/doi/10.1002/aelm.201600353/abstract>. This article may be used for non-commercial purposes in accordance with Wiley Terms and Conditions for Self-Archiving (<http://olabout.wiley.com/WileyCDA/Section/id-828039.html#terms>).

All material supplied via Aaltodoc is protected by copyright and other intellectual property rights, and duplication or sale of all or part of any of the repository collections is not permitted, except that material may be duplicated by you for your research use or educational purposes in electronic or print form. You must obtain permission for any other use. Electronic or print copies may not be offered, whether for sale or otherwise to anyone who is not an authorised user.

This is the pre-peer reviewed version of the following article:

M. Malitckaya, H.-P. Komsa, V. Havu, and M.J. Puska, *Advanced Electronic Materials* **2017**, 3, 1600353.
DOI: 10.1002/aelm.201600353

First-principles modelling of point defects and complexes in thin-film solar-cell absorber CuInSe_2

*Maria Malitckaya, Hannu-Pekka Komsa, Ville Havu, Martti J. Puska**

Maria Fedina 1, Dr. Hannu-Pekka Komsa 1, Dr. Ville Havu 1, Prof. Martti J. Puska 1

Department of Applied Physics, Aalto University, P.O. Box 11000, Espoo, Finland.

E-mail: martti.puska@aalto.fi

Keywords: CuInSe_2 , solar cell, native point defects, density functional theory

2/16/2017

Point defects and complexes may affect significantly physical, optical, and electrical properties of semiconductors. The Cu(In,Ga)Se_2 (CIGSe) alloy is an absorber material for low-cost thin-film solar cells. Several recently published computational investigations show contradicting results for important point defects such as copper antisite substituting indium (Cu_{In}), indium vacancy (V_{In}), and complexes of point defects in CuInSe_2 . In the present work we study effects of the most important computational parameters especially on the formation energies of point defects. Moreover, related to defect identification by the help of their calculated properties we discuss possible explanations for the three acceptors, which occur in photoluminescence measurements of Cu-rich samples. [S. Siebentritt *et al.*, *Progress in Photovoltaics: Research and Applications* **2010**, 18, 390, S. Siebentritt *et al.*, *physica status solidi (c)* **2004**, 1, 2304.] Finally, new insight into comparison between theoretical and experimental results is presented in the case of varying chemical potentials and of formation of secondary phases.

1. Introduction

The chalcopyrite Cu(In,Ga)Se_2 (CIGSe) alloy is a promising candidate for low-cost flexible thin-film photovoltaic solar cells. Efficiencies of solar cells using CIGSe as the light absorber are steadily increasing thanks to detailed investigation of device parameters.^[1, 2, 3] The defect microstructure influences optical and electronic properties of the absorber material. Understanding its evolution during the manufacturing and during the solar cell operation is impossible without knowledge of the fundamental parameters of point defects in CIGSe or eventually in its parent materials CuInSe_2 and CuGaSe_2 .

Experimentally, valuable information on point defects in semiconductors can be obtained especially from photoluminescence (PL) measurements or Hall measurements. Composition-dependent PL measurements and Hall measurements have been performed on chalcopyrite CIGSe by Siebentritt *et al.*^[4, 5] For example, close to the stoichiometric compound, PL measurements showed three acceptor levels with ionization energies of 40 meV, 60 meV, and 100 meV above the valence band maximum (VBM) and one donor level 10 meV below the conduction band minimum (CBM).^[4] The intensities of these three peaks vary, as the composition of the sample changes from Cu-rich to Cu-poor, so that in the Cu-poor samples only one peak is detected. Although only the Cu-poor material is important for actual devices Cu-rich samples give indispensable information for defect identification.

First-principles calculations based on the density functional theory (DFT) can be used to obtain important, complementary information about point defects such as formation energies and charge transition levels.^[6] A plethora of studies concerning defects in CuInSe_2 and CuGaSe_2 has been published over the last two decades.^[7-13] The most recent DFT investigations have employed hybrid functionals, which can overcome the energy band gap problem plaguing the older studies

and can thus also provide information about the defect level positions within the band gap. ^[9, 10, 11, 12, 13] The results of different calculations agree well with respect to general trends in formation energies of the most important defects, such as the copper vacancy (V_{Cu}), indium antisite on copper place (In_{Cu}), and copper interstitial (Cu_{int}). However, the results differ in some important cases. For instance, there are clearly different values for the ionization levels within the band gap for the copper antisite on the indium place (Cu_{In}) and indium vacancy (V_{In}). Based on the formation energy calculations, V_{Cu} and Cu_{In} are abundant acceptors, and are most probably responsible for some of the above-mentioned PL peaks, but it is unclear whether any native defect can be responsible for the third acceptor level.

One important goal of the present work was to gain a perspective on the present unsatisfactory situation in modelling point defects in CIGSe and to approach the ultimate accuracy by which DFT is able to predict the properties of bulk crystalline materials. ^[14] First we carried out a detailed benchmarking of the first-principles computational scheme used. We checked effects due to the supercell size and shape, as well as those of the finite-size supercell correction scheme. We used also two very different implementations of the first-principles DFT method, which differ in describing valence-core electron interaction and electron wave functions (see below). After finding the computational parameters yielding accurate results, we calculated formation energies and charge transition levels for different acceptor candidates in CuInSe_2 . By carefully considering the relevant chemical potential limits, we were able to draw conclusions about the abundances of different defects. In addition to simple native defects, we have also considered a set of complexes formed by them. Our paper is organized as follows. Computational parameters and methods are described in Sec. II. In Sec. III we discuss the chemical potential limits and present a detailed benchmarking related to the supercell size and shape. Our results for defect formation energies are presented in Sec. IV. Finally, in Sec. V we discuss which defects could be abundant acceptors on

the basis of our first-principles results and compare our findings with the above-mentioned PL spectra.

2. Computational methods

Most of the calculations of this work were carried out in the framework of DFT with the VASP program package ^[15, 16] based on the projector-augmented wave (PAW) method ^[17] and the use of the plane-wave basis set. In our calculations the plane-wave cutoff energy was 455 eV which was determined by a convergence test for the total energy of pristine CuInSe₂. In order to improve electronic and atomic structures and to get a realistic energy band gap necessary for formation energy calculations, we used the hybrid exchange-correlation functional HSE06 (Heyd-Scuseria-Ernzerhof). ^[18] We used the default parameters for the portion of the Hartree-Fock exchange ($\alpha=0.25$) and for the inverse screening length $\omega=0.20 \text{ \AA}^{-1}$, in order to have an unbiased comparison with previously published results obtained by different tunings of the α and ω parameters for reproducing the experimental CuInSe₂ band gap. Relaxation of ionic positions were continued until forces on each atom fell below 0.01 eV/Å. The ensuing structural parameters for the bulk CuInSe₂ show good agreement with the experimental results and the band gap is in line with previous theoretical results; see Table 1 for comparison.

Table 1. Calculated and measured lattice constants a and c and energy band gap E_g for CuInSe₂. The lattice parameters correspond to the tetragonal 16-atom unit cell.

	$a \text{ (\AA)}$	$c \text{ (\AA)}$	$E_g \text{ (eV)}$
Present work	5.78	11.64	0.90
Exp.1 ^{a)}	5.81	11.63	1.04
Exp.2 ^{b)}	5.76	11.54	1.04

a) [19], b) [20]

We modeled point defects by using a large number of different supercell sizes and shapes (see Results section). The defect formation energy E_f is defined as ^[6,21]

$$E_f = E_{tot}^{defect} - E_{tot}^{bulk} - \sum_i n_i \mu_i + q E_F + E_{corr}, \quad (1)$$

where E_{tot}^{defect} is the total energy of the supercell containing the defect, E_{tot}^{bulk} the total energy of the bulk supercell, μ_i the chemical potential of the atom of type i , n_i the number of added atoms when creating the defect in the supercell, q the charge state of the defect, and E_F is the Fermi level measured from the VBM.

E_{corr} is an energy correction term accounting for the errors due to the finite size of the supercell. These errors arise mainly from the electrostatic interaction of a charged defect with its periodic images and with the neutralizing background charge. ^[22] Other sources of errors are the elastic interactions between the defect and its periodic images. Various correction schemes have been proposed for the electrostatic finite-size error correction for charged defects, e.g., those by Makov and Payne (MP), ^[23] Lany and Zunger (LZ), ^[24] and by Freysoldt, Neugebauer, and Van de Walle (FNV). ^[25] The MP method is not suitable if the defect state is not well localized. ^[23] In contrast, the FNV scheme is general so that it can be easily applied to systems with any supercell shapes and even when the dielectric tensor is anisotropic, which is the case for CuInSe₂. To this end, the FNV scheme was mainly used in the present article, but we also compare its results to those of the LZ scheme in the case of the tetragonal supercell.

In all of these correction schemes, dielectric constants of the host materials are required to evaluate, how the interactions between charges are screened. Our values, calculated using the HSE06 functional, are presented in Table 2. Since CuInSe₂ is tetragonal, the dielectric constants

along the a and c directions differ slightly. Our values are in a good agreement with experimental values of 11.3^[26] and 13.6.^[27] The potential alignment term of the FNV correction is determined along the c -direction and thus a static dielectric constant of 11.15 is used.

Table 2. Calculated macroscopic dielectric tensor. ϵ_∞ and ϵ_{ion} are the electronic and ionic contributions to the dielectric tensor. The static dielectric constant ϵ_0 is the sum of the two contributions.

Direction	ϵ_∞	ϵ_{ion}	ϵ_0
a,b	7.86	2.53	10.40
c	7.86	3.29	11.15

Finally, when considering complexes of point defects the binding energy E_b of a defect complex AB is defined as

$$E_b^{AB} = E_f^{AB} - (E_f^A + E_f^B), \quad (2)$$

where E_f^A , E_f^B , and E_f^{AB} are the formation energies of the defects A and B and that of the complex AB, respectively, and they have to be calculated for the same values of the Fermi-level and the chemical potentials.

3. Point defects

3.1 Chemical potential stability diagram

From the thermodynamic point of view, the phase stability diagram determines the regions of the chemical potentials, where a particular compound will be stable. In case of CuInSe_2 , the chemical potential diagram is based on the formation enthalpies $\Delta H_f(\text{X})$ of different binary and ternary compounds (X). Their values, based on the PBE and HSE06 calculations for all of the considered

phases, are presented in Table 3 together with the respective experimental values. Further computational details are given in Appendix A.

Table 3. Formation enthalpies ΔH_f (eV) calculated using the PBE and HSE06 functionals as well as the corresponding experimental values.

Compound	PBE	HSE06	Experiment
CuSe	-0.27	-0.45	-0.42 ^{a)}
In ₂ Se ₃	-2.45	-2.99	-3.57 ^{a)}
CuInSe ₂	-1.77	-2.40	-2.12 ^{a)} , -2.77 ^{b)}
Cu ₂ Se	0.01	-0.65	-0.42 ^{a)}
InSe	-1.05	-1.28	-1.22 ^{a)}
CuIn ₅ Se ₈	-7.08	-8.93	—

a) [28] b) [29]

Using the formation enthalpies, the stability diagram for CuInSe₂ can be constructed by determining the lowest energy phase at the given chemical potential values. The resulting stability diagram for the copper-indium-selenium system is shown in Figure 1. The chemical potentials are given in the form $\mu_i = \mu_i^0 + \Delta\mu_i$, where $\Delta\mu_i$ is the deviation from the chemical potential in the stable elemental phase (μ_i^0). When using this definition it is required, in order to avoid precipitation of elemental phases, that $\Delta\mu_i \leq 0$. Within the diagram region where CuInSe₂ is the most stable phase, the chemical potentials satisfy

$$\mu_{Cu} + \mu_{In} + 2\mu_{Se} = \Delta H_f(CuInSe_2). \quad (3)$$

We note that the stability diagram is strictly speaking valid only under the thermodynamic equilibrium.

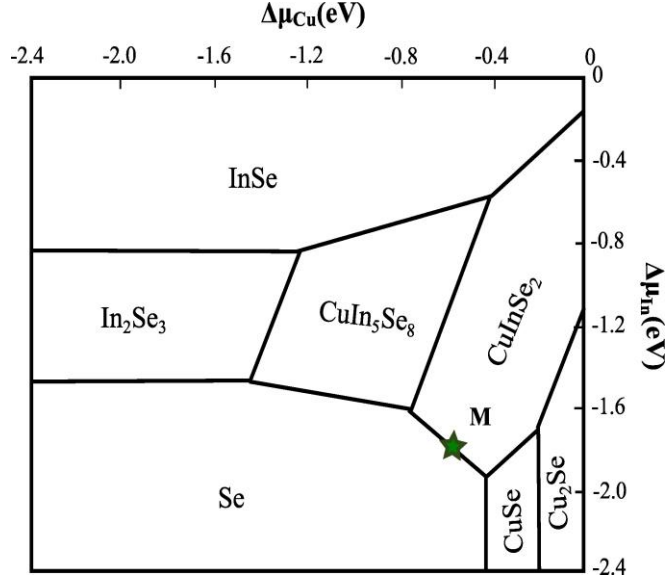


Figure 1. Stability diagram for CuInSe₂ constructed using the heats of formation calculated with the HSE06 functional and presented in Table III. Point M correspond to point A in Figure 1 in the paper by Pohl and Albe^[9] and it is used in comparisons below.

Chemical potential diagrams for CuInSe₂ have been presented in many previous articles.^[24, 7, 9, 11, 13] Generally, they agree qualitatively, but in some cases the CuInSe₂ stability regions may differ remarkably from the other results, even among those calculated using the HSE06 functional. Our phase stability diagram is close to that calculated by Yee *et al.*^[13] and also to those presented by Pohl and Albe^[9], Huang *et al.*^[12] or Kim *et al.*^[30] Due to a differing CuInSe₂ heat of formation, the chemical potential diagram by Bekaert *et al.*^[11] has a noticeably bigger stability region than that in the present work.

3.2 Supercell shape and size

We first focus on describing the effect of the chalcopyrite supercell shape and size used in the calculations. Supercells constructed both from the 16-atom tetragonal unit cell [lattice vectors $(a, 0, 0)$, $(0, a, 0)$, and $(0, 0, c)$, $c \approx 2a$]^[9, 12, 13] and from the 8-atom triclinic primitive cell [lattice vectors

$(a,0,0)$, $(0,a,0)$, and $d=(a/2,a/2,c)$, $c \approx a$, $|d| \approx 1.22a$] have been employed in the previous studies. ^[11],

^{10]} Various possible supercells with their properties are listed in Table 4.

Table 4. Supercells of different sizes for the chalcopyrite lattice. The 8-atom primitive unit cell is triclinic(tric) and the 16-atom unit cell tetragonal(tetr).

Size	Unit cell	Supercell size	Lengths of supercell lattice vectors
32	tric	2x2x1	2a, 2a, 1.22a
64	tetr	2x2x1	2a, 2a, 2a
64	tric	2x2x2	2a, 2a, 2.44a
128	tetr	2x2x2	2a, 2a, 4a
144	tric	3x3x2	3a, 3a, 2.44a
144	tetr	3x3x1	3a, 3a, 2a
216	tric	3x3x3	3a, 3a, 3.67a
288	tric	3x3x4	3a, 3a, 4.88a
432	tetr	3x3x3	3a, 3a, 6a
512	tetr	4x4x2	4a, 4a, 4a
512	tric	4x4x4	4a, 4a, 4.88a

According to Oikkonen *et al.*, even the 32-atom supercell is sufficient for obtaining converged formation energies for neutral defects. ^[10] On the other hand, in the case of charged defects, spurious interactions between a defect and its images converge extremely slowly as a function of the supercell size. However, these errors can be corrected by using finite-size correction schemes.

To illustrate the magnitude of these errors, the uncorrected and the FNV corrected formation energies for the the unrelaxed $\text{In}_{\text{Cu}}^{+2}$ defect are shown in Figure 2. Here, an unrelaxed defect was considered in order to study only the effects of electrostatic interactions between the defect and its periodic images and to avoid other interactions arising, e.g, from long-range strain fields. In order to access also large supercell sizes, a smaller plane-wave cutoff energy of 300 eV was used. Both tetragonal and triclinic supercells were adopted. Since the supercells are of different shape, we cannot perform a straightforward extrapolation to the limit of the infinite supercell volume. However, it is clear from the figure that the uncorrected formation energies undergo large variations, whereas the corrected ones are nearly independent on the supercell size. Moreover, the uncorrected energies approach the corrected ones from below, as expected for localized charges in supercells reasonably close to the cubic shape. ^[22]

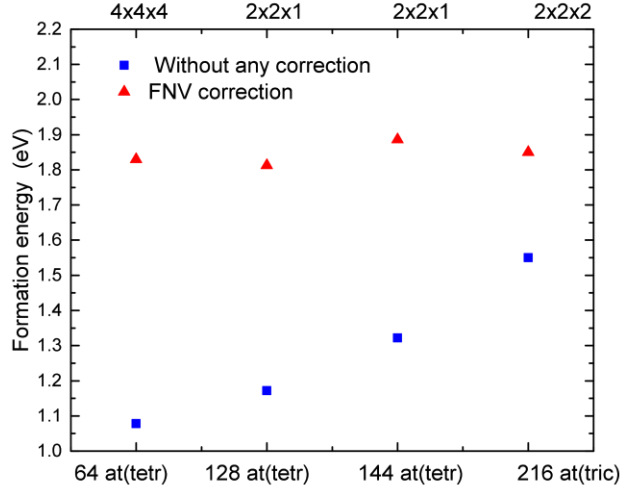


Figure 2. Formation energy of the $\text{In}_{\text{Cu}}^{+2}$ antisite for different supercell shapes and sizes. Values for the unrelaxed defects are compared. k-points sets used for the chosen supercell sizes are shown on the top of plot. The chemical potentials correspond to point M in Figure 1 and the Fermi level is at the VBM.

Next, as a more realistic test case we show in Figure 3 the formation energy diagram for the relaxed Cu_{In} antisite calculated using different supercells and the FNV correction. Here, in order to show the performance of even larger supercells, results for the 432-atom supercell are included. They are calculated using the FHI-aims code^[31] and employing the HSE06 functional. FHI-aims is an all-electron code in which electron wavefunctions are presented in the efficient basis of numerical atomic orbitals and in which the accuracy can be systematically improved by extending the basis set.^[31] Thus, performing calculations by FHI-aims allows us also to verify whether the results depend on the basis set or the description of the core states. According to Figure 3 the absolute values of the formation energies and, consequently, also the charge transition levels, show only minor variations for supercells larger than 64 atoms, irrespective on the electronic-structure method used. It has been found that the 64-atom supercell cannot correctly accommodate localized states in the band gap near the band edges.^[9] This may be the main reason for the deviation of the 64-atom supercell results from the other, better-converged ones in Figure 3. In contrast, it is gratifying to note that the 128-atom supercell performs well in spite of its highly rectangular shape with 90 degree angles (See Table 4). The reason is that the defect charge - neutralizing background charge interaction has decreased between the 64- and 128-atom supercells in addition to the increase of the defect-defect distance along the c-direction of the lattice.

In previous investigations, the LZ scheme has often been adopted for the finite-size correction. In Figure 4, different correction schemes are compared. Since the LZ scheme is difficult to use for arbitrary supercell shapes, we carried out these calculations for the tetragonal 64-atom supercell. As already found out in previous studies,^[22] the LZ scheme tends to yield smaller corrections than the FNV scheme. However, in the present case, the corrected results are rather similar.

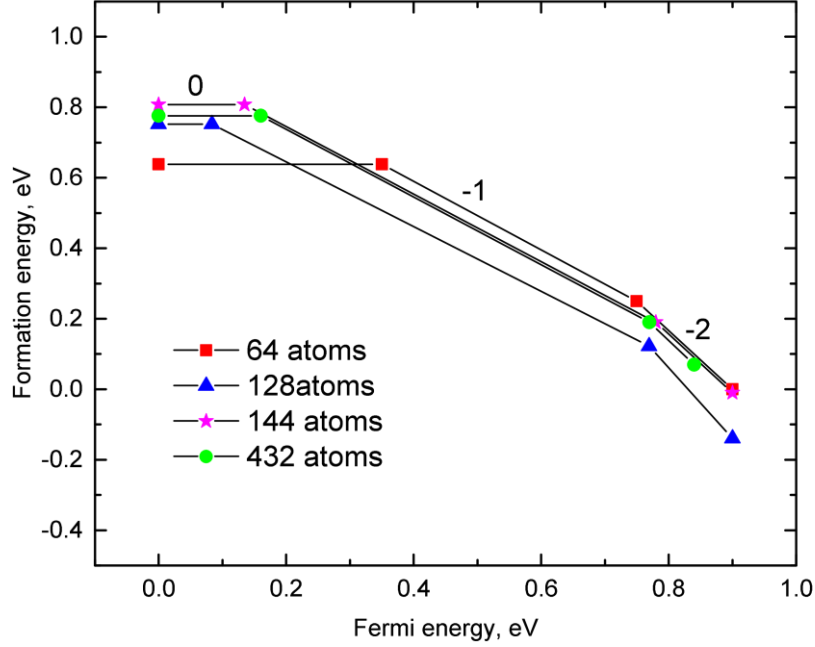


Figure 3. Formation energy of the Cu_{In} antisite as a function of the Fermi level obtained using the 64, 128, and 144 -atom supercells and the VASP code, as well as the 432-atom supercell and the FHI-aims code.

The chemical potentials correspond to point M in Figure 1.

In conclusion, the FNV and LZ schemes give similar results when the defect charge is well-localized within the supercell. The FNV scheme can be easily applied for arbitrary supercell shapes allowing the use of the smallest supercells fulfilling this requirement. This may be crucial for obtaining adequate results in the case of several charged defects.

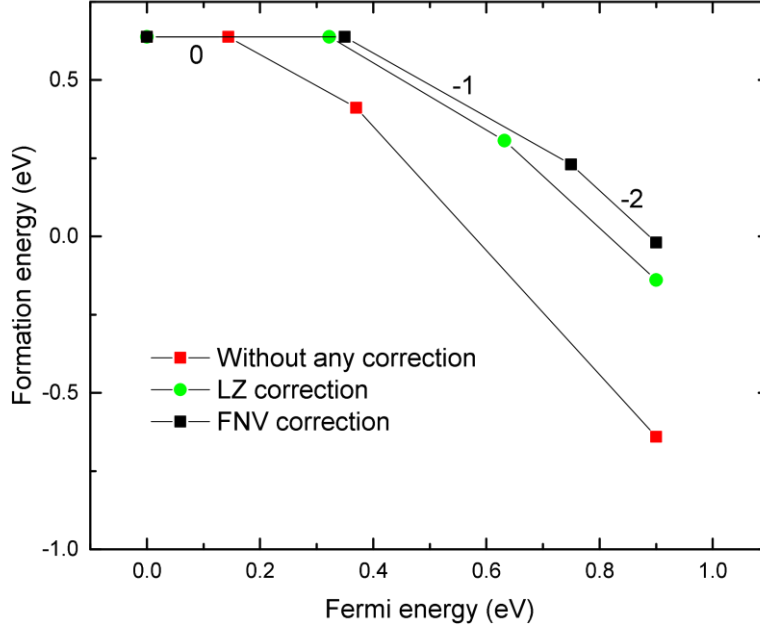


Figure 4. Formation energy of the Cu_{In} antisite as a function of the Fermi level. The calculations are performed with the 64-atom supercell and with different correction schemes. The chemical potentials correspond to point M in Figure 1.

4. Defect formation energies

On the basis of the benchmarks in the previous section, we adopted the 128-atom supercell and the $2 \times 2 \times 1$ k-point set for all further defect calculations. The high-efficiency Cu-poor CIGSe absorbers are prepared under a selenium-rich atmosphere.^[32] The experimental conditions correspond to the boundary between the CuInSe_2 and Se stability regions in the stability diagram (Figure 1). Therefore, point M in Figure 1 was chosen for the chemical potentials when calculating the defect formation energies. This corresponds to $\Delta\mu_{\text{Cu}} = -0.5$ eV and $\Delta\mu_{\text{In}} = -0.87$ eV. The resulting

formation energies are shown in Figure 5 for all the simple low-formation-energy point defects considered in this work as a function of the Fermi level. The numerical data on the formation energies at the same chemical potential conditions and the Fermi level at the VBM are listed in Table 5 for all relevant charge states. Defects which have in the formation energy plots a negative charge at the VBM are shallow acceptors and defects becoming negative slightly above the VBM are deeper acceptors.

Table 5. Defect formation energies in CuInSe₂ (eV). The chemical potentials correspond to the point M in Figure 1 and the Fermi level is at the VBM.

Point defect	-3	-2	-1	0	+1	+2	+3
V _{Cu}	—	—	0.84	0.88	—	—	—
V _{In}	3.37	2.63	2.32	2.23	—	—	—
Cu _{In}	—	1.66	0.89	0.75	0.83	1.24	—
In _{Cu}	—	—	—	2.94	—	0.72	—
Cu _{int}	—	—	4.02	1.98	0.77	—	—
In _{int}	—	—	—	5.21	8.03	3.52	2.93
V _{Se}	—	—	—	2.25	—	—	—

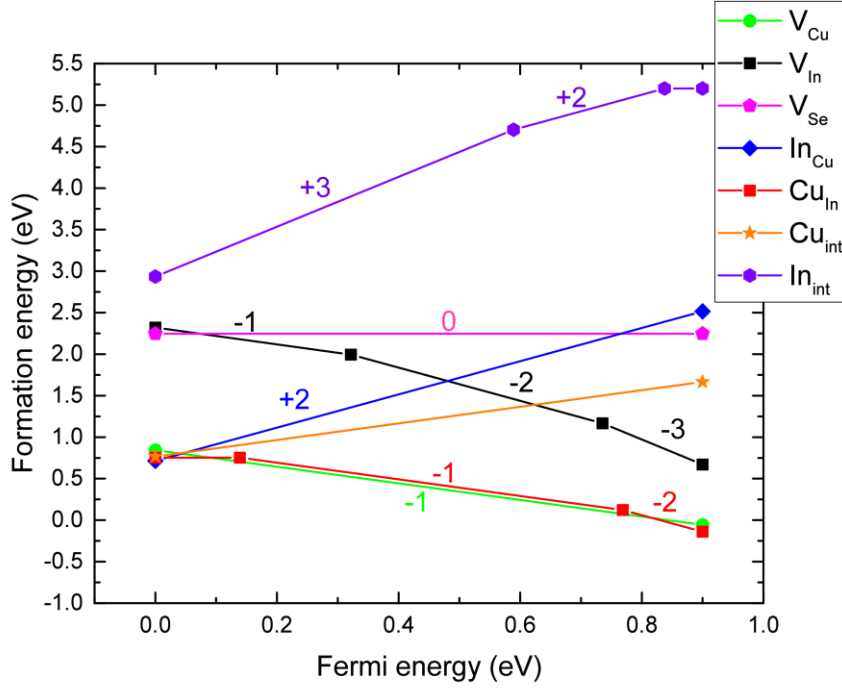


Figure 5. Defect formation energies in CuInSe₂ as a function of the Fermi level. The chemical potentials correspond to point M in Figure 1.

Our results for the formation energies, when evaluated at the same chemical potentials, are in close agreement with those calculated by Yee *et al.*^[13] and Pohl and Albe.^[9] Especially, we also found two charge transition levels within the band gap for Cu_{In} and two acceptor levels for V_{In}. The small shifts in the transition levels between different works can be explained by different supercell sizes and different finite-size correction schemes used. Furthermore, our calculated energy band gap is about 0.1 eV smaller than the experimental one (1.04 eV, Table 1). In some works, the parameters α and ω of the HSE06 functional have been tuned to yield a band gap closer to the experiment. This will naturally result in small shifts in the transition level positions with respect to the band edges, but the effect on the formation energies is very small.^[33] Oikkonen *et al.*^[10] and Bekaert *et al.*^[11] did not report on transition levels for Cu_{In} and V_{In} at all, in contrast to

our results and to those by Yee *et al.*^[13], by Huang *et al.*^[12], as well as to those by Pohl and Albe^[9]. In comparison with other results, those by Huang *et al.*^[12] showed the strongest tendency toward deep states inside the band gap, which may reflect the largest Hartree-Fock exchange fraction of 30% used in their HSE06 functional calculations. Increasing this fraction results in more localized single-electron states. According to our defect formation energies, Cu-rich and Se-rich material will be p-type with the the most important acceptors being V_{Cu} and Cu_{In} and the most important donors being Cu_{int} and In_{Cu} . Cu_{In} is predicted to be a deeper acceptor than V_{Cu} because its transition level from the neutral to the singly negative state is inside the band gap. However, we should bear in mind that the accuracy of first-principles calculations for the transition levels is of the order of 0.1 eV. The conclusion about the most abundant acceptors and donors is in agreement with the results by Lany *et al.*,^[24] by Pohl and Albe,^[9] by Huang *et al.*,^[12] and Yee *et al.*,^[13] as well as with those by Oikkonen *et al.*^[10] Due to the above-mentioned larger CuInSe_2 stability region, Bekaert *et al.*^[11] found also V_{In} as an abundant acceptor.

5 Acceptor candidates

5.1 Point defects

The formation energies and hence the concentrations of the native defects depend strongly on the chemical potentials used in the calculations. Experimentally this is manifested by the different numbers of PL peaks seen in Cu-poor and Cu-rich samples. To find out which of the native defects are likely to form at sufficiently large concentrations to be visible in PL measurements, we calculated the formation energies at chemical potential values relevant to the experimental conditions.

The line in Figure 6 shows the chemical potential values considered. Point A corresponds to extremely Cu-rich material and point F to extremely Cu-poor material. Due to the Se excess in a typical CuInSe₂ growth, we consider conditions close to the Se phase boundary. When growing stoichiometric or Cu-rich CuInSe₂ one has to increase the copper concentration and then remove Cu₂Se precipitates from the alloy.^[34] This experimental condition can be associated with the Cu₂Se stability region in Figure 6. On the other hand, high-quality solar cell absorber material is often Cu-poor.^[35] Moreover, a larger Cu deficiency is observed at grain surfaces, where the material can start forming so-called ordered defect compounds (ODC). Point E is taken to model such conditions.

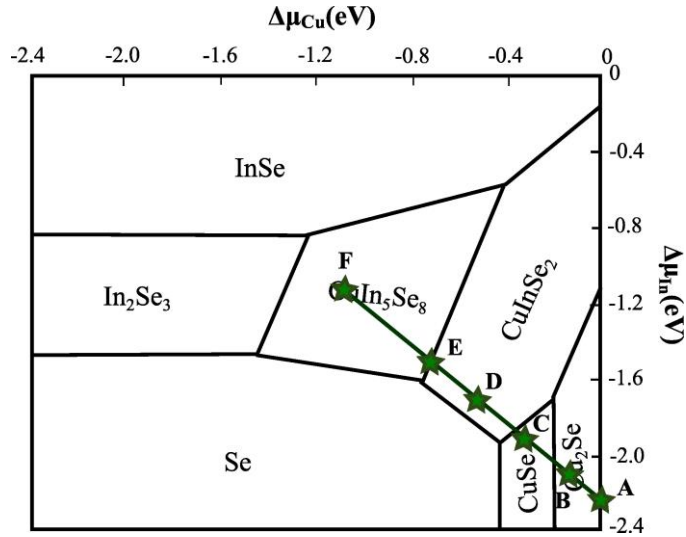


Figure 6. Chemical potential diagram. The stars, connected by a straight line, correspond to the equilibrium states discussed in the text.

Formation energies, corresponding to the above-defined range of chemical potentials, are presented in Figure 7 for the most important point defects, as a function of the In chemical potential. The solid and dashed lines in the figure correspond to the acceptor and donor defects, respectively. Even throughout this extended range of chemical potentials V_{Cu} and Cu_{In} are the

acceptors of the lowest formation energies, irrespective of the Fermi-level position. Especially, for p-type material (E_F at the VBM) there are no other acceptors with competitive formation energies. Accounting also for the donors, the Cu-rich region between points A and B is characterized by a large concentration of Cu_{In} and Cu_{int} defects, and the Cu-poor region between points E and F by that of V_{Cu} and In_{Cu} defects.

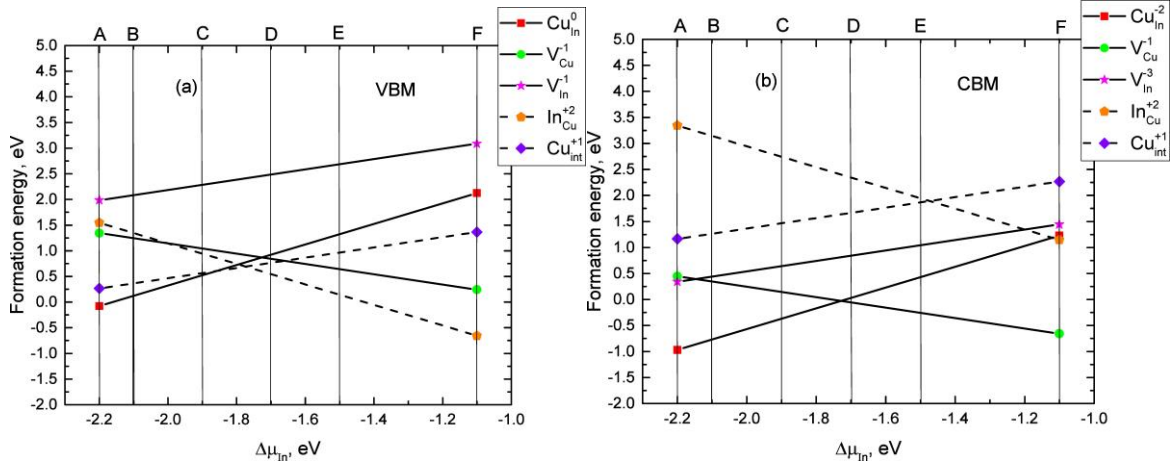


Figure 7. Point defect formation energies along the green line in stability diagram of Figure 6. The energies are calculated for E_F at (a) VBM and (b) CBM. The dashed and solid lines correspond to the donor and acceptor defects, respectively.

Within the Cu-rich region between points A and B and for n-type doped samples, the formation energy of the acceptor-type V_{In} is low and close to that of V_{Cu} . However, the other two abundant defects, V_{Cu} and Cu_{In} , are also acceptors and thus n-type doping under these conditions is unlikely. Indeed, while highly Cu-poor samples were found to be n-type due to the formation of In_{Cu} defects, stoichiometric and Cu-rich samples were p-type.^[36] It is remarkable that in the p-type material (Figure 7 a) both of the correlated defects, Cu_{int} and V_{Cu} , are among those of the lowest formation energies even in Cu-rich material. This reflects the weak Cu-Se bonds^[8] and the small ionic radius of the Cu ion. Moreover, because Cu_{In} is neutral when the Fermi level is close to the VBM and the

formation energy of In_{Cu} is high in the In-poor material, Cu_{int} and V_{Cu} form a correlated pair also due to charge neutralization. Naturally, the formation of the Cu_{In} and Cu_{int} defects in large quantities will eventually lead to the precipitation of CuSe and Cu_2Se .

In summary, based on our formation energy studies the native point defects considered so far can undoubtedly account for only two acceptor defects, V_{Cu} and Cu_{In} . To extend our search, we next investigate several defect complexes.

5.2 Defect complexes

Point defects in CuInSe_2 can form different complexes. Complexes comprising copper vacancies, such as $\text{In}_{\text{Cu}}\text{-V}_{\text{Cu}}$, $\text{V}_{\text{Se}}\text{-V}_{\text{Cu}}$, $\text{In}_{\text{Cu}}\text{-2V}_{\text{Cu}}$, and the antisite-related defect $\text{In}_{\text{Cu}}\text{-Cu}_{\text{In}}$, have been considered in the literature.^[9, 10, 37] The complex $\text{V}_{\text{Se}}\text{-V}_{\text{Cu}}$ was suggested to explain an observed metastability.^[8] The $\text{In}_{\text{Cu}}\text{-2V}_{\text{Cu}}$ complex is important because it will be abundant in Cu-poor p-type material and it is suggested to be the basic building block in the ODCs.^[37] However, the binding energies calculated by Pohl and Albe indicate fairly weak bonding.^[9] Moreover, $\text{In}_{\text{Cu}}\text{-2V}_{\text{Cu}}$ is neutral and $\text{In}_{\text{Cu}}\text{-V}_{\text{Cu}}$ singly positive for all the Fermi level positions in the band gap so that they cannot act as acceptors. The formation energy of the neutral V_{Se} is relatively high (Figure 5) so that $\text{V}_{\text{Se}}\text{-V}_{\text{Cu}}$ is not expected to be abundant in Se-rich growth conditions.

The most stable complexes should be made up of both acceptors and donors feeling a strong Coulomb attraction. Moreover, complexes that could behave as acceptors obviously require acceptor(s) of a (total) charge negative enough so that it is not compensated by the positive charge contributed by the donor(s). This is also the reason why we have not considered, in spite of the low formation energy, $\text{In}_{\text{Cu}}^{+2}$ as a part of a complex. $\text{In}_{\text{Cu}}^{+2}$ would require several native point defect acceptors in order to make a complex into an acceptor. Because defect complexes are formed by aggregation of native defects the abundance of the constituent native defects is crucial for the

abundance of a defect complex. Thus, we chose to study the complexes $\text{Cu}_{\text{int}}-2\text{V}_{\text{Cu}}$, $\text{Cu}_{\text{int}}-\text{V}_{\text{In}}$, and $\text{Cu}_{\text{int}}-\text{Cu}_{\text{In}}$. Their binding energies are listed in Table 6.

As discussed above, the concentrations of Cu_{int}^+ and V_{Cu}^- are high in p-type Cu-rich material. Thus, during the growth process their agglomeration to complexes is expected to be very probable. For example, Cu_{int}^+ can be coupled with two V_{Cu}^- vacancies to form the acceptor complex $(\text{Cu}_{\text{int}}-2\text{V}_{\text{Cu}})^-$. Its binding energy is minimized when Cu_{int}^+ locates between the two V_{Cu}^- vacancies giving $E_b = -0.36$ eV for all the Fermi level positions in the band gap (the complex and its constituents have only one charge state, Figures 5 and 8). This is not a strongly bound complex, but taking into account the abundance of its constituents its existence is plausible.

Table 6. Binding energies of defect complexes (eV) in the different charge states.(See Fig.

Error! Reference source not found.)

Point defect	-2	-1	0	+1
$\text{Cu}_{\text{int}}-2\text{V}_{\text{Cu}}$	—	-0.36	—	—
$\text{Cu}_{\text{int}}-\text{V}_{\text{In}}$	-0.91	-0.65	-0.65	—
$\text{Cu}_{\text{int}}-\text{Cu}_{\text{In}}$	—	-0.70	-0.33	-0.33

We have also considered the complex $\text{Cu}_{\text{int}}-\text{V}_{\text{In}}$, because, although the formation energy of V_{In} is relatively high, it is anyway lowered toward Cu-rich - In-poor material, especially if the material becomes less p-type. Because the charge state of V_{In} varies from -1 to -3 when the Fermi level rises in the band gap the complex may act as an acceptor, when V_{In} is in the -2 or -3 charge state. The nearest-neighbor configuration is impossible for this complex, because the copper interstitial fills easily the vacant indium place and produces an antisite. However, the second nearest-neighbor configuration is rather strongly bound with $E_b = -0.65$, -0.65, and -0.91 eV for the 0, -1, and -2

charge state, respectively, and for the Fermi level at the beginning of the stability region of each charge state. The -1 charge state will become stable when the Fermi level rises 0.1 eV above the VBM indicating a rather shallow acceptor character. As the point defect V_{In} has three possible charge states in the band gap (Figure 5), complexes comprising V_{In} also have three charge states (Figure 8). However, the positions of the corresponding transition levels are not the same. Due to the high binding energy of the -1 charge state, the transition level (0/-1) has shifted toward the VBM and the (-1/-2) transition level toward the CBM in comparison with the transition levels (-1/-2) and (-2/-3) for V_{In} , respectively.

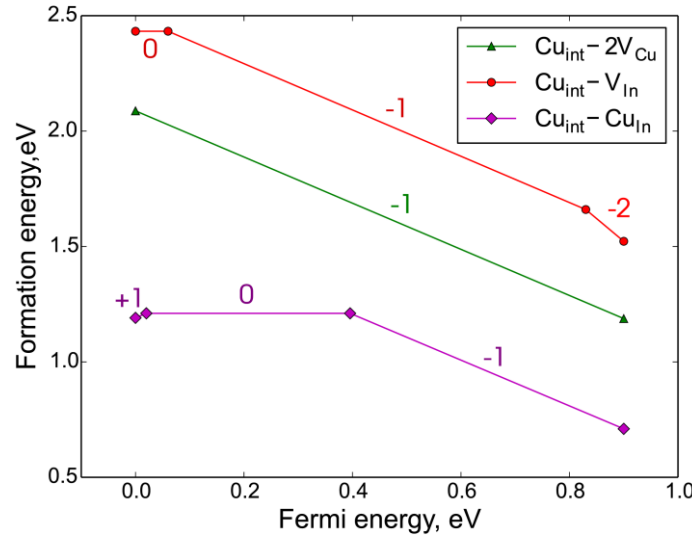


Figure 8. Formation energies of defect complexes as a function of the Fermi level at point M on the stability chemical potential diagram of Figure 1.

A possible candidate for an abundant acceptor is also $Cu_{int}-Cu_{In}$. This complex will be stable in Cu-rich conditions. Also its charge state varies as a function of the Fermi level in the band gap (Figure 8). When the Fermi level is close to the VBM, this complex is stable in the +1 charge state with a binding energy of -0.33 eV. The complex ($Cu_{int}-Cu_{In}$) has a binding energy of -0.33 eV and

it is stable for E_F in the middle of the band gap. In n-type materials, when E_F is close to the CBM, the acceptor defect $(\text{Cu}_{\text{int}}\text{-Cu}_{\text{In}})^{-1}$ will be stable with the lowest binding energy of -0.70 eV. The transition levels of $\text{Cu}_{\text{int}}\text{-Cu}_{\text{In}}$ are shifted relatively to those of Cu_{In} (Figure 8). Notice, that the shift of the transition level is larger when the difference between the binding energies of the two charge states is larger.

In summary, from all the defect complexes considered, $\text{Cu}_{\text{int}}\text{-2V}_{\text{Cu}}$, $\text{Cu}_{\text{int}}\text{-V}_{\text{In}}$, and $\text{Cu}_{\text{int}}\text{-Cu}_{\text{In}}$ could act as acceptors. However, the predicted binding of $\text{Cu}_{\text{int}}\text{-2V}_{\text{Cu}}$ is relatively weak. The relatively high formation energy of V_{In} lowers its abundance as well as that of $\text{Cu}_{\text{int}}\text{-V}_{\text{In}}$. The complex $\text{Cu}_{\text{int}}\text{-Cu}_{\text{In}}$ could act as an acceptor only in n-type material. These notions shed some doubts on the importance of only native defect complexes as acceptors in CuInSe_2 . Finally, the thermal equilibrium concept and the use of defect formation energies are doubtful for determining complex abundances. Therefore a conclusive study would also require the study of the kinetics of the native point defects which is beyond the scope of the present study.

6. Conclusions

Discrepancies in theoretical calculations can often be associated with the choice of computational parameters. In the case of compound semiconductors, such as the ternary compound CuInSe_2 the choice of the chemical potential sets is the most important problem, because it strongly affects the values of the formation energies and hence the concentrations of point defects and defect complexes. However, the chemical potentials do not influence the existence and positions of the transition levels.

The finite-size problem for the electrostatic energy of charged defects in semiconductors and insulators can be solved by different correction schemes. Our calculations for native point defects

in CuInSe₂ show that the most popular schemes give qualitatively and quantitatively comparable results. However, defect formation energies can depend on the wave function overlap or elastic interactions between defects in neighboring supercells. We have calculated formation energies for supercells comprising up to 432-atoms. Our results show that the 128- and 144-atom supercells are sufficient to resolve the properties of the most important defects in CuInSe₂.

The growth conditions for CuInSe₂ can vary from Cu-poor to Cu-rich. The actual growth parameters affect the abundances of the different types of point defects. In the present study we varied the chemical potentials to their extreme values to model different growth conditions. In a p-type material the shallow acceptor V_{Cu} , the slightly less shallow acceptor Cu_{In} , and the shallow donors Cu_{int} and In_{Cu} are predicted to coexist as abundant defects over a relatively wide range of chemical potentials. The concentrations of V_{Cu} and In_{Cu} increase toward Cu-poor conditions and those of Cu_{int} and Cu_{In} toward Cu-rich conditions.

Our results show that the native point defects V_{Cu} and Cu_{In} are clearly responsible for two of the acceptors seen in PL measurements in Cu-rich conditions. Of these, V_{Cu} is abundant also in Cu-poor conditions. The question about the third acceptor present in Cu-rich conditions is more subtle. Among the possible candidates the relatively high formation energy of V_{In} even in In-poor conditions makes it less abundant and the stability, abundance, or the deep-acceptor character of the defect complexes, such as $Cu_{int}-2V_{Cu}$, $Cu_{int}-V_{In}$, and $Cu_{int}-Cu_{In}$, may question also their role as the third acceptor.

Acknowledgment

The project has received funding from the European Union Horizon 2020 research and innovation program under the grant agreement No 641004. HPK also thanks the Academy of Finland for the support under Project No. 286279, and through its Centres of Excellence Programme (2012-2017)

under Project No. 251748. We acknowledge the generous computational resources provided by CSC supercomputer center of Finland and also by the Aalto Science-IT project. We also like to thank Prof. S. Siebentritt of the University of Luxembourg for discussions of the PL results.

References

- [1] P. Jackson, R. Wuerz, D. Hariskos, E. Lotter, W. Witte, and M. Powalla, *physica status solidi (RRL) - Rapid Research Letters* **2016**, 8, 583.
- [2] P. Jackson, D. Hariskos, R. Wuerz, W. Wischmann, and M. Powalla, *physica status solidi (RRL) - Rapid Research Letters* **2014**, 8, 219.
- [3] P. Jackson, D. Hariskos, R. Wuerz, O. Kiowski, A. Bauer, T. M. Friedlmeier, and M. Powalla, *physica status solidi (RRL) - Rapid Research Letters* **2015**, 9, 28.
- [4] S. Siebentritt, M. Igalson, C. Persson, and S. Lany, *Progress in Photovoltaics: Research and Applications*, **2010**, 18, 390.
- [5] S. Siebentritt, N. Rega, A. Zajogin, and M. C. Lux-Steiner, *physica status solidi (c)* **2004**, 1, 2304.
- [6] C. Freysoldt, B. Grabowski, T. Hickel, J. Neugebauer, G. Kresse, A. Janotti, and C. G. Van de Walle, *Reviews of Modern Physics* **2014**, 86, 253.
- [7] C. Persson, Y.-J. Zhao, S. Lany, and A. Zunger, *Phys. Rev. B* **2005**, 72, 035211.
- [8] S. Lany and A. Zunger, *Phys. Rev. B* **2005**, 72, 035215.
- [9] J. Pohl and K. Albe, *Phys. Rev. B* **2013**, 87, 245203.
- [10] L. E. Oikkonen, M. G. Ganchenkova, A. P. Seitsonen, and R. M. Nieminen, *Journal of Physics: Condensed Matter* **2014**, 26, 345501.
- [11] J. Bekaert, R. Saniz, B. Partoens, and D. Lamoen, *Phys. Chem. Chem. Phys.* **2014**, 16, 22299.
- [12] B. Huang, S. Chen, H. X. Deng, L. W. Wang, M. A. Contreras, R. Noufi, and S. H. Wei, *IEEE Journal of Photovoltaics* **2014**, 4, 477.
- [13] Y. S. Yee, B. Magyari-Köpe, Y. Nishi, S. F. Bent, and B. M. Clemens, *Phys. Rev. B* **2015**, 92, 195201.
- [14] K. Lejaeghere, G. Bihlmayer, and T. Björkman, *Science* **2016**, 351, 6280.
- [15] G. Kresse and J. Furthmüller, *Phys. Rev. B* **1996**, 54, 11169.
- [16] G. Kresse and J. Furthmüller, *Computational Materials Science* **1996**, 6, 15.
- [17] P. E. Blöchl, *Phys. Rev. B* **1994**, 50, 17953.
- [18] J. Heyd, G. E. Scuseria, and M. Ernzerhof, *The Journal of Chemical Physics* **2003**, 118, 8207.
- [19] H. W. Spiess, U. Haeberlen, G. Brandt, A. Ruber, and J. Schneider, *physica status solidi (b)* **1974**, 62, 183.
- [20] W. Paszkowicz, R. Lewandowska, and R. Bacewicz, *Journal of Alloys and Compounds* **2004**, 362, 241.
- Proceedings of the Sixth International School and Symposium on Synchrotron Radiation in Natural Science (ISSRNS).
- [21] C. G. Van de Walle, D. B. Laks, G. F. Neumark, and S. T. Pantelides, *Phys. Rev. B* **1993**, 47, 9425.
- [22] H.-P. Komsa, T. T. Rantala, and A. Pasquarello, *Phys. Rev. B* **2012**, 86, 045112.
- [23] G. Makov and M. C. Payne, *Phys. Rev. B* **1995**, 51, 4014.
- [24] S. Lany and A. Zunger, *Modelling and Simulation in Materials Science and Engineering* **2009**, 17, 084002.
- [25] C. Freysoldt, J. Neugebauer, and C. G. Van de Walle, *physica status solidi (b)* **2011**, 248, 1067.
- [26] M. V. Yakushev, F. Luckert, C. Faugeras, A. V. Karotki, A. V. Mudryi, and R. W. Martin, *Applied Physics Letters* **2010**, 97, 152110.
- [27] P. W. Li, R. A. Anderson, R. H. Plovnick, *Journal of Physics and Chemistry of Solids* **1979**, 40, 333.
- [28] D. Cahen and R. Noufi, *Journal of Physics and Chemistry of Solids* **1992**, 53, 991.
- [29] A. S. Verma, S. Sharma, and V. K. Jindal, *International Journal of Modern Physics B* **2012**, 26, 1250079.
- [30] N. Kim, P. P. n. Martin, A. A. Rockett, and E. Ertekin, *Phys. Rev. B* **2016**, 93, 165202.
- [31] V. Blum, R. Gehrke, F. Hanke, P. Havu, V. Havu, X. Ren, K. Reuter, and M. Scheffler, *Computer Physics Communications* **2009**, 180, 2175.
- [32] F. Pianezzi, P. Reinhard, A. Chirila, B. Bissig, S. Nishiwaki, S. Buecheler, and A. N. Tiwari, *Phys. Chem. Chem. Phys.* **2014**, 16, 8843.
- [33] H.-P. Komsa, P. Broqvist, and A. Pasquarello, *Phys. Rev. B* **2010**, 81, 205118.
- [34] R. Noufi, R. Axton, C. Herrington, and S. K. Deb, *Applied Physics Letters* **1984**, 45, 668.
- [35] S. Siebentritt, L. Gtay, D. Regesch, Y. Aida, and V. Depurand, *Solar Energy Materials and Solar Cells* **2013**, 119, 18.
- [36] C. Stephan, S. Schorr, M. Tovar, and H.-W. Schock, *Applied Physics Letters* **2011**, 98, 091906.
- [37] S. B. Zhang, S.-H. Wei, and A. Zunger, *Phys. Rev. Lett.* **1997**, 78, 4059.

